Tutors

Dr. Ángel Morales García
Departament de Ciència de Materials i Química Física

Dr. Francesc Viñes Solana
Departament de Ciència de Materials i Química Física

Grau de Química

Treball Final de Grau

Single-Atoms Catalysts based on MXenes
Catalitzador d'àtoms metàl·lics aïllats basats en MXenes

Sara Pibernat Cabañas

January 2021

Universitat de Barcelona

B:KC Barcelona Knowledge Campus
Campus d'Excel·lència Internacional

Research is to see what everybody else has seen,
and to think what nobody else has thought.

Albert Szent-Györgyi

Primer de tot, agrair als meus dos tutors, Ángel i Francesc, per tot el suport i l'ajuda al llarg d'aquest treball, gràcies a ells he obtingut els coneixements necessaris per dur a terme aquest treball de fi de grau, també mencionar els meus familiars i amics pel suport emocional i la motivació que m'han donat en els moments més complicats d'aquest treball.

REPORT

CONTENTS

1. SUMMARY

Heterogeneous catalysis is crucial on the development of chemical products in industrialized societies. A great deal of major industrial chemical transformations involves heterogeneous catalysts, which are typically comprised of transition metals and metal oxides as substrates. Two-dimensional metastable transition-metal carbides and nitrides, known as MXenes, have garnered increasing attention for nearly a decade because of their versatile composition and structure, stability under certain conditions of interest in catalysis, and numerous appealing properties.

The synthesis of Singe-atom Catalyst (SACs) is one of the main active areas in heterogeneous catalysis with the ultimate goal of promoting small-size metal particles as Sisngle Atoms (SAs). Thus, the search for appropriate substrate for SACs is highly demanded for the next generation of heterogeneous catalysis.

The present study aims at introducing low-dimensional transition metal carbides as feasible substrates for anchoring single metal atoms by using first-principles based on density functional theory (DFT), calculations. In particular, we focussed on the 4*d* transition metal atoms (TMs) and nine bare MXene surfaces with M_2C stoichiometry (M= Ti, V, Cr, Zr, Nb, Mo, Hf, Ta, and W). The adsorption energies of four different active sites were studied to find the most stable site, H_M, and the situation where the SA isolation would be thermodynamically favourable. This energetic parameter is used to find a correlation with respect to structural features such as the atomic height over the MXene surface, the MAX exfoliation energies, and by comparing 4*d* with 3*d* TMs. In addition, few TMs from Pt-group plus Au are also investigated in this project. The results show, shortly, that Pt and Au are better dispersed than Pd and Ag and all the 5*d* TMs are more prone to be isolated with the V_2C MXene.

Keywords: MXenes, Heterogeneous catalysis, Single-atom catalysts, Density Functional Theory, Adsorption energies.

2. RESUM

La catàlisi heterogènia és crucial en el desenvolupament de productes químics en les societats industrialitzades. Un dels gran reptes són les transformacions químiques on intervé la catàlisi heterogènia. Hi ha carburs i nitrurs de metalls de transició bidimensionals i metaestables, també anomenats MXenes, que durant una dècada han sigut el focus d'atenció a causa de la seva versàtil composició i estructura, la seva estabilitat sota condicions d'interès com la catàlisi, i nombroses altres propietats atractives.

La síntesi de catalitzadors d'àtoms aïllats (*Singel Atoms Catalysts* - SACs) és una de les àrees principals en la catàlisi heterogènia amb l'objectiu final d'obtenir petites partícules metàl·liques en la forma d'àtoms aïllats (*Single Atoms* - SAs) . Per tant, la recerca de substrats apropiats pels SACs és molt important per la següent generació de catalitzadors heterogenis.

El present estudi intenta introduir carburs de metalls de transició de petites dimensions com a substrats vàlids per ancorar àtoms metàl·lics aïllats emprant càlculs de primers principis basats en la teoria funcional de la densitat (DFT). En concret, ens centrarem en els metalls de transició (*Transition Metals* - TMs) de la sèrie 4*d* i nou MXenes nets amb la estequiometria M_2C (M= Ti, V, Cr, Zr, Nb, Mo, Hf, Ta, i W).L'energia d'adsorció de quatre diferent llocs actius ha estat estudiada per trobar el lloc més estable; el H_M, i per trobar la situació on l'aïllament del SA sigui termodinàmicament favorable. Aquest paràmetre energètic ha estat emprat per trobar una correlació respecte característiques estructurals com l'alçada atòmica sobre de la superfície del MXene, l'energia d'exfoliació de la fase MAX, i per comparar els TMs dels períodes 4*d* i 3*d*. Addicionalment, uns quants TMs del grup del Platí més el Au han sigut investigats en aquest projecte. Com a resum, el Pt i el Au estan millor dispersats que el Pd i el Ag, i per altra banda, tots els TMs de la sèrie 5*d* són més propensos de trobar-se aïllats amb el MXene V_2C.

Paraules clau: MXens, Catàlisi heterogènia, Catalitzadors d'àtoms aïllats, Teoria funcional de la densitat, Energies d'adsorció.

3. INTRODUCTION

One of the clearest definitions of catalysis was given by Wilhelm Ostwald, who stated it as *"the acceleration of a slow chemical process by the presence of a foreign material, which is not consumed"*.[1] More than a century later, catalysis contributes to more than 37% of the world Gross Domestic Product (*GDP*).[2] The majority of industrial catalytic processes involve heterogeneous environments constituted by: A solid foreign material or catalyst, and reactants in the gas and/or liquid phase. Transition metals, metal oxide-based materials, and zeolites are among the most widely used material in heterogeneous catalysis, although transition-metal sulphides, nitrides, carbides, phosphates, phosphides, even ion-exchange resins, and clays are also employed for some particular applications. [3,4]

Recently, a fast-growing family of two-dimensional (2D) transition metal carbides, nitrides, and carbonitrides, usually referred as MXenes, have gained great interest since the discovery of the first Ti_3C_2 MXene in 2011.[5] These MXenes have been successfully isolated by selective etching using hydrofluoric acid (HF) from MAX bulk phase precursors, which are composed by an early transition metal, M, a metal of the *d*-block, A, and either carbon or nitrogen denoted by X.[5,6] Since the M-A chemical bonds are weaker than the M-X ones, the formation of MXenes are feasible by using selective etchants.[8] The resulting 2D flake materials have been fully characterized being made up of closed-packed layers of transition metals, *e.g.* M = Ti, V, Cr, Zr, Nb, Mo, Hf, Ta, and W, intercalated by, for instance, layers of carbon, *i.e.* X = C, with the general formula $M_{n+1}X_nT_x$, for n =1, 2, and 3, where T_x represents the surface functionalization bonded to the outer M layers. Clearly, these terminations depend on the employed etchants and the subsequent chemical treatment, and these are usually terminated with surface groups such as F, OH, H or O.[1,7]

The great number of possible MXenes, in terms of composition, makes possible the tailoring of the MXenes properties by selecting the M and X elements, the number of atomic layers in the sheet, and the type of surface terminations. Focusing on the later one, a recent work has shown that the surface termination can be removed or substituted in a rational, predetermined way, further expanding the MXene universe and their possible applications, including bare MXenes.

These ones have generated a great expectation in several fields like photocatalysis,[9] energy storage,[10] heterogeneous catalysis,[6,12] electrocatalysis,[7,13] and charge storages.[13,14]

One of the latest applications for MXenes is their use as suitable substrates for creating Single-Atom Catalysts (*SACs*).[2,6,11,12] The idea is to generate specific active sites at the substrate surface, where single metal atoms get anchored. Pt/FeO_x was the first SAC synthetized with a noted catalytic performance.[11,12] Compared to traditional catalysts, SACs exhibit the advantages of both homogeneous and heterogeneous catalysts, in terms of improvement in specific activity and reduction in the amount of loaded noble metals.[7] Trough high performance computing and sophisticated electronic structure methods, many theoretical efforts have been devoted to design efficient SACs, and ascribed their high chemical activities to the SAC low-coordination number, and its electronic polarization, which translates into strong metal-molecule interactions.[13] The SACs catalytic activity and selectivity do not only depend on the nature of the Single-Atom (*SA*), but also on the solid supports that are used to disperse these SA. Therefore, an appropriate support is essential to ensure strong interactions between the isolated SACs and substrate, so to avoid the adatoms aggregation. [9]

The main goal of the present project is to investigate the capability of bare MXenes, with stoichiometry M_2C M= Ti, V, Cr, Zr, Nb, Mo, Hf, Ta, and W, to form SACs by first-principles calculations assessment. This has been initially done for a list of *4d* Transition Metals (*TMs*) Y, Zr, Nb, Mo, Tc, Ru, Rh, Pd, Ag, and Cd, see Figure 1, thus following an earlier study carried out on *3d* TMs. As will be explained below, other late TMs of the *5d* series, these are, the Pt-group metals Os, Ir, and Pt, plus Au, have been studied as well, which provides a general overview of the possibilities of such MXenes in dispersing the studied TMs, as done previously on graphene,[15] likely to be done thanks to their metastability, and also observed on *e.g.*, graphyne.[16] The spotlight is placed on finding trends on the possible dispersion, here seized from a thermodynamic point of view, comparing the adsorption energies to the corresponding TMs bulk cohesive energies.

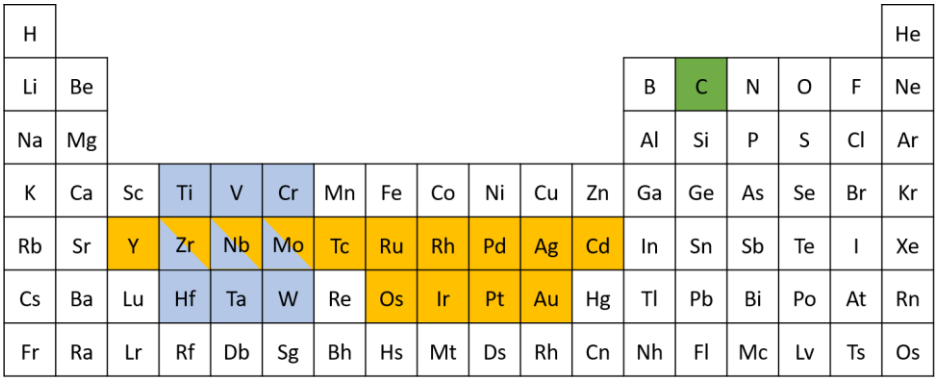

Figure 1.View of the Periodic Table with the elements that compose the investigated TM@MXene, highlighted in colour, including the early TM components, M, the explored 4*d* and 5*d* TM adatoms, and carbon as X, shown in blue, orange, and green, respectively.

4. OBJECTIVES

The aim of this research project is to analyze the interaction of single 4*d* metal atoms (Y, Zr, Nb, Mo, Tc, Ru, Rh, Pd, Ag, and Cd) on bare MXenes with M2C stoichiometry (M= Ti, V, Cr, Zr, Nb, Mo, Hf, Ta, and W) that operate as substrates with the ultimate goal of proposing potential single atom catalysts (SACs). To shed light on this concern, the following particular goals will be addressed:

- To evaluate the adsorption energies considering all possible combinations between single metal atoms and MXenes, so as to identify most stable adsorption sites.
- To identify the influence of a particular single metal atom over MXenes and that of a MXene over the single metal atom.
- To ascertain the M@MXene situations where the SA isolation would be thermodynamically favourable.
- To correlate the adsorption energies with respect the atomic height over the surface and the MAX exfoliation energies, the latter generated from Al-derived MAX precursor phase.
- To acquire trends of the possible SAC formation along MXene groups and series, as well as along the 4*d* series.
- To compare such trends for the 3*d* and the 4*d* adatoms.
- To finally evaluate the trends on Pt-group, plus Au, compared to the 4*d* cases.

5. THEORETICAL BACKGROUND

5.1. QUANTUM CHEMISTRY

During the last part of the XIX Century, many scientists believed that all the fundamental discoveries of science had been made, and so little remained to be discovered. Indeed, during the early XX Century they just established the laws of the macroscopic world related to the movement of objects, referred to as classical mechanics. However, when travelling towards nanoscale world, one can observe that the classical mechanics does not properly works. There, the laws of the nature are governed by Quantum Mechanics. This field of physics is the extension of classical ideas projected into the behaviour of subatomic, atomic, and molecular species. Hence, our current understanding of the atomic structure and molecular bonding derived from terms of the fundamental principles of quantum mechanics, and no understanding of chemical systems is possible without knowing the basics of this current theory of matter.

During the last few decades, Quantum Mechanics suffered an explosive growth, thanks to the availability of highly parallelized supercomputing facilities placed in the hands of investigation, which allowed to routinely carry out atomistic and molecular calculations permitting the prediction of results and its synergistically union with experiments.

5.1.1. Schrödinger Equation and Born-Oppenheimer Approximation

A chemical system can be defined as a matter which consist of many particles in an arbitrary initial state. All observable properties of the quantum system can be predicted from its wavefunction solving the Schrödinger equation.[14]

$$\hat{\mathrm{H}} = \hat{T}_e + \hat{T}_n + \hat{V}_{ee} + \hat{V}_{en} + \hat{V}_{nn} \qquad \text{(Eq. 1)},$$

where $\hat{T}_e$ and $\hat{T}_n$ are the kinetic energy operators of the *e* electrons and *n* nuclei, respectively, whereas $\hat{V}_{ee}$, $\hat{V}_{nn}$, and $\hat{V}_{en}$ stand for the coulomb repulsion among electrons, nuclei, and the attraction between electrons and nuclei, respectively.[19]

The problem resides in that the Schrödinger equation can be only analytically solved for very simple systems, called hydrogenous atoms, when there is only one electron. As soon as, two electrons repel each another, one cannot figure out the electrostatic potential. This prompted of different approximations to obtain veridic results.[17]

When one assumes that nuclei and the electrons are punctual masses, while spin-orbit interactions and other relativistic interactions can be disregarded, the time-independent Hamiltonian operator, $\hat{\mathrm{H}}$, can be expressed as the sum of kinetic and coulombic operators.

The wavefunctions and the energies of a chemical system in a stationary state are obtained from the time-independent Schrödinger equation:

$$\hat{\mathrm{H}}\Psi_{(q_i,q_\alpha)} = E\Psi_{(q_i,q_\alpha)} \qquad \text{(Eq. 2)},$$

where q_i and q_α correspond to the electronic and the nuclear coordinates, respectively. The resolution of these equations requires some approximations so as to be solvable. The first one is the well-known Born-Oppenheimer Approximation (*BOA*),[23] that sustains on the fact that nuclei are far heavier than electrons. Hence, the electrons move much faster than nuclei, so nuclei can be considered as static. Here, it must be pointed out that the internuclear distances are not a variable, and they are fixed to a constant value every time a calculation is done.[19,20] So, the Schrödinger equation just has the electronic coordinates as variables and the contribution of the nuclei repulsion is a constant value. Knowing this and decoupling the different terms, the Schrödinger equation gets reduced to solving the electronic contribution $\hat{\mathrm{H}}_e$:

$$\hat{\mathrm{H}}_e = \hat{T}_e + \hat{V}_{ee} + \hat{V}_{en} \qquad \text{(Eq. 3)},$$

Another inconvenience that must be taken into account is the interaction between electrons in polyelectronic systems. In a many-electron system, one needs to include the electron repulsion in the potential energy term or the wave-equation.[18] There are two main approximations used following a variational principle, named as Hartree-Fock (*HF*) based methods, including all the

plethora of post-HF methodologies, and the Density Functional Theory (*DFT*).[18] The former method requires a whole set of single-particle wave functions to calculate the single-electron potential, making it, from scratch, more computationally expensive for the analysis of systems like bulk or surface models. On the contrary, modern implementations of DFT can provide much higher accuracy than HF calculations at a lower computational cost. This theory reduces the problem of calculating the ground state of a many-electron system as the properties of the system can be determined considering a unique functional of the ground state with a single electron density. The low computational cost of DFT has led to a steady increase in the use of DFT for the study of larger molecules and systems of different kinds.[20]

5.1.2. Density Functional Theory

The DFT rests on two fundamental mathematical theorems proved by Hohenberg and Kohn,[22] plus the derivation of a set of equations by Kohn and Sham.[18]

The first theorem proved that the ground-state energy from the Schrödinger equation is a unique functional of the electron density. It states that it exists a one-to-one mapping between the ground-state wave function and the ground-state electron density. It is based on defining the system energy as a functional, *i.e.,* a function of a function, in this case, the electron density function, $\rho(\mathrm{r})$.

$$F[f] = \int_{-1}^{1} \rho(\mathrm{r}) \qquad \text{(Eq. 4)},$$

where $F[f]$ is the functional of the function $\rho(\mathrm{r})$. In such a way, the system energy can be expressed as $E[\rho(\mathrm{r})]$. Another way to interpret Hohenberg and Kohn theory is establishing that the ground-state electron density uniquely determines all properties, including the energy and the wave-function, of the ground state. This leads us to solve the Schrödinger equation by finding a function of three spatial variables, the electron density, rather than a function of 3*N* variables, and the wave function, where *N* is the number of particles in the system.[20]

Although this theorem rigorously proves that a functional of the electron density exists and it can be used to solve the Schrödinger equation, the theorem says nothing about what the function actually is. The second theorem defines another property of the functional known as the Kohn-Sham potential: The electron density that minimizes the energy of the overall functional is the true

electron density corresponding to the full solution of the Schrödinger equation. This variational principle is used in practice with approximated forms of the functional.

A useful way to write down the functional described by the Hohenberg-Kohn theorem is in terms of the single-electron wave functions, $\phi_i(r)$, and therefore, the energy functional can be written as $E[\phi_i(r)]$,[20,22] which can be split into a collection of terms that can be written down in a simple analytical form:

$$E[\rho] = T[\rho] + E_{ne}[\rho] + E_{ee}[\rho] + E_{nn}[\rho] + E_{xc}[\rho] \qquad \text{(Eq. 5)},$$

where the terms are, in order, the electronic kinetic energy, $T[\rho]$, the Coulombic interactions between electrons and nuclei, $E_{ne}[\rho]$, the Coulombic interaction between pairs of electrons, $E_{ee}[\rho]$, the Coulombic interaction between pairs of nuclei, $E_{nn}[\rho]$, and the exchange-correlation functional, $E_{xc}[\rho]$. This last one is defined to include all the quantum mechanical effects that are not included in the other terms.

The results taken from Hohenberg and Kohn theorems show that the sought ground state can be found by minimizing the energy of an energy functional, and that this can be achieved by finding a self-consistent solution to a set of single-particle equations. However, the rock-in-the-shoe to solve Kohn-Sham equations is that one has to specify the exchange-correlation function.[19,20]

5.1.3. Exchange-Correlation Functionals

Although a priori the formulation of the DFT theory is exact, all complexities of the many-body problem are cast into an unknown object, referred to as the exchange-correlation (*xc*) functional, E_{xc}. This is a crucial term, which has to be approximated, though. Consequently, the success or failure of DFT calculations rests solely on the validity of the chosen approximation to the *xc* functional.[24]

It follows from Eq. 5 that the E_{xc} has contributions from various factors such as the kinetic correlation energy, T_c, which is the difference between the kinetic energy of the real system and a reference system of noninteracting electrons, plus contains the self-interaction correction as well, the exchange energy, and the coulombic correlation energy. Thus, E_{xc} not only accounts for the difference between the classical and quantum mechanical electron-electron repulsion, but

it also includes the kinetic energy difference between the fictious noninteracting system and the real system. Even if this contribution is very small and sometimes neglected, in certain cases is key and should be accounted for.[20,22]

A uniform electron gas model provides a practical way to use the Kohn-Sham equations by setting the *xc* potential at each position to be that xc potential of the electron density. Such derived *xc* functionals are called to be within the Local Density Approximation (*LDA*),[22] as it uses only the density function as a variable to approximate the *xc* functional. Another improvement is the Generalized Gradient Approximation (*GGA*),[25] which includes the density gradient in its calculations as a variable. Because there are many ways in which information from the gradient of the electron density can be included in a GGA functional, there are many distinct GGA functionals. Two of the most widely used in calculations involving solids are the Perdew-Wang functional (*PW91*),[26] and the Perdew-Burke-Ernzerhof functional (*PBE*)[27].

Further improvements can be gained when including the electron density second derivative as an E_{xc} variable, in the so-called meta-GGA *xc* functionals. Finally, more complex *xc* functionals are the hybrids, which include a portion of the HF exchange in the mathematic expression. In the present study, the GGA-PBE *xc* functional is used, as known to be good in describing the energetic of transition metal carbide bulk and surfaces,[28] and also of MXene systems.[29]

5.2. Bloch Theorem and Periodic Systems

Crystalline solids are inherently periodic. This feature permits the simplification of the computational cost, reducing their description to a simple unit cell, which represents the extended solid in a three-dimensional space. On the other hand, the construction of two-dimensional models has the additional requirement of including a vacuum perpendicular to the material surface in order to avoid interaction between translationally repeated models defined within a three-dimensional periodic cell.[30]

Aside, Bloch theorem applies to the electronic wave-functions inside a crystal, and rests in the fact that the Coulomb potential in a crystalline solid is also periodic. This theorem enables the use of a unit cell to describe the properties of an infinite system.[31] A peculiarity of this method is that the system described by this wavefunction is not defined in the real space, but in its reciprocal

one. Both spaces are inversely connected, meaning, in practice, that a short distance is in the real lattice corresponds to a long one in the reciprocal space, and *vice versa*.

5.3. MXENE STRUCTURES

The MXene materials are synthesized by selective chemical etching from MAX phases, as reported by the literature.[32] For instance, the Ti_3AlC_2 compound, the MAX phase most used in MXene synthesis, is treated with HF to extract the Aluminium layers, and, after sonication to separate the layers, the 2D Ti_3C_2 is gained.[19] It has been pointed out that the etching conditions are harsher for those MAX phases displaying larger exfoliation energies,[32,33] understood as a form of surface tension or as the energy required to peel off an atomic layer from the surface of a bulk material, in this case, the A layers needed to be removed to gain the MXene material. In this sense, it is also related to the bond strength between the A layers and the MXene units.[29]

MXenes offer periodicity only on the two possible material directions. However, when using three-dimensional cells, due to the use of periodic boundary conditions, the total height of the cell, in the direction perpendicular to the plane of the MXene slab, is set to a value that can ensure at least 10 Å of vacuum width between the periodic copies of the cell, even after adsorbing a small molecule,[23] known to be enough to avoid interaction in between translationally repeated slabs, see Figure 2.

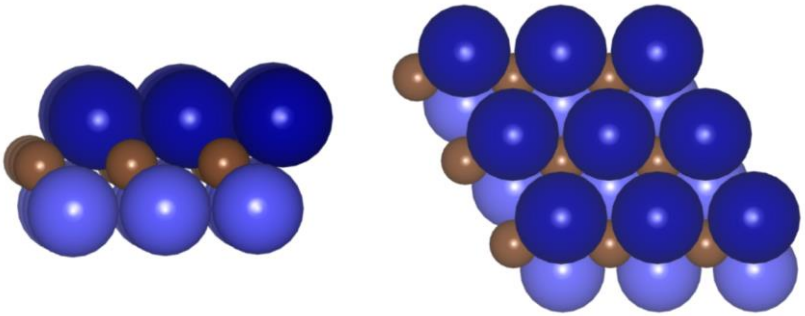

Figure 2. Side (left) and top (right) views of a M_2C MXene. M and C atoms are shown as blue and brown spheres, respectively.

It is worth pointing out that many of the studies done with MXenes describe a real situation involving terminated MXene substrates.[34] This is not surprising since after its synthesis, or under ambient conditions MXenes can become oxidized.[29,35] However, as posed in this study, the

possible application in catalyst also allows inducing the oxygen depletion over the $M_{n+1}X_nO_n$ through the cleaning by annealing at 700 ºC and exposing the resulting surface to H_2 gas flow.[35] This variation can facilitate the process of obtaining single atoms by having 2D structures with metal carbon bonds (M–C), which are weaker compared to the metal oxygen bonds (M–O) in typical oxide supports.

A total of nine MXenes with M_2X stoichiometry M= Ti, Zr, Hf, V, Nb, Ta, Cr, Mo, and W for TMs from groups IV–VI were selected to investigate the adsorption energy of different 4*d* and 5*d* adatoms at four different high-symmetry position of the MXene (0001) basal plane surface of bulk Transition Metal Carbide (*TMCs*) with rocksalt structure.[30] For these TMCs, the (111) surfaces have considerable higher surface energy than the most stable (001) one.[36] In accordance, MXenes are predicted to be quite chemically active, while permit to investigate surfaces that could hardly exist in bulk TMCs otherwise.

Concerning the adsorption sites of MXenes for the explored TM adatoms, four different high symmetry sites are studied, labelled top site (T) where the adatom is placed above a M surface atom, the bridge site (B), where the adatom is above the surface in the midpoint of a M-M bond, and two kinds of three-fold hollow sites, having either a metal or a carbon underneath, H_M and H_C, respectively, see Figure 3.

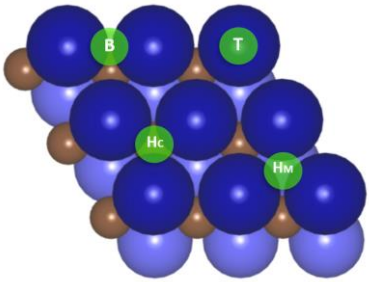

Figure 3.Top view of an employed *p*(3×3) MXene supercell, with tags detailing the explorer adsorption sites coloured in green, including top (T), bridge (B), three-fold hollow site with a subsurface metal atom (H_M), and a three-fold hollow site with an underlying C atom (H_C). Colour coding as in Figure 2.

5.4. ENERGETIC ASSESSMENTS

5.4.1. Adsorption Energy

For each studied adatom, MXene substrate, and site, the adsorption energy is calculated, so as to quantify the adsorption strength of the adatom metal on the (0001) MXene surface. For any adsorption energy, E_{ads}, is defined as:

$$E_{ads} = -[E_{TM/MXene} - (E_{MXene} + E_{TM})] \quad \text{(Eq. 6)},$$

where $E_{TM/MXene}$ is the total energy of the MXene layer with the TM adatom attached, E_{MXene} is the total energy of the bare MXene (0001) surface, and E_{TM} the total energy of the isolated metal atom.[7,34] This way the resulting adsorption energies are defined positive, this is, the larger the E_{ads} value, the stronger the interaction between MXene and the adatom.[4]

It is well-known that any of the standard *xc* approximations do not include a description of dispersive forces, *e.g.,* like van der Waals (*vdW*). These forces are normally only relevant for intermolecular situations; however, their inclusion always improves the description. To account for it, one needs to add a proper correction.[36] Some examples are the popular Grimme D3 correction.[37] developed nonlocal van der Waals functionals (*vdW-DF*),[38] even the accurate Many-Body Dispersion (*MBD*).[39] All these corrections have been thoroughly tested and successfully applied on a huge of different systems, including inter- and intramolecular cases starting from rare gases to large graphene sheets. The first mentioned correction, Grimme D3, has been found to be one of the best choices for the interaction of MXene surfaces with adatoms.[40]

5.4.2. Cohesive Energy

The cohesive energy, E_{coh}, can be regarded as the energy that must be supplied to a solid to separate its atomic constituents into neutral free at rest and at infinite separation. From another point of view, it can be regarded as the released energy when such atoms cluster to form the solid. As far as SACs are concerned, the E_{coh} can be used to assess whether there is a thermodynamic preference towards isolating or clustering. This can be done by calculating the difference energy, in between E_{ads} and E_{coh}, so:

$$E_{diff} = E_{ads} - E_{coh} \quad \text{(Eq. 7)},$$

In general, a positive E_{diff} implies that the adatoms are more stable, *i.e.,* stronger bound, when being dispersed adatoms on the substrate, compared to bulk environments. *Vice versa*, when E_{diff} is negative, the TM atoms are more stable in a bulk environment, being this a driving force towards clustering. The cohesive energies were already calculated with the same computational setup as in the present work, and available in the literature.[41]

6. COMPUTATIONAL DETAILS

The present spin-polarised DFT calculations were carried out using the Vienna *Ab initio* Simulation Package (*VASP*),[34] using the PBE *xc* functional,[38] but also including the Grimme D3 dispersion interaction description.[39] The core electrons were described using Projector Augmented Wave (*PAW*)[42] pseudopotentials, and the valence electron density was expanded in a plane wave basis set with a cutoff energy of 415 eV. The geometry optimizations were considered converged when the forces acting in the nuclei were all below 0,01 eV· $Å^{-1}$, with an electron convergence criterion of 10^{-6}eV. A tetrahedron smearing of 0.2 eV width has been used to speed up electronic convergence, yet total energies have been extrapolated to zero smearing, *i.e.*, zero Kelvin. All atoms were allowed to relax during the optimizations.

In order to avoid interactions between replicated MXenes, the total height of the cell, in the direction perpendicular to the plane of the MXene slab, is set to 16 Å, thus ensuring at least 10 Å of vacuum width between the periodic copies of the cell, even after adsorbing a small molecule. To sample the necessary numerical integrations in the reciprocal space, Monkhorst-Pack ***k***-points 5×5×1 and 1×1×1 grids were used for the MXenes and the isolated TM atoms, respectively. These latter were thus calculated Γ-point in an asymmetric cell of 9×10×11 Å dimensions.

7. RESULTS AND DISCUSSION

In this section, the results based on the interaction of the 4*d* transition metal atoms (TM= Y, Zr, Nb, Mo, Tc, Ru, Rh, Pd, Ag, and Cd); from now on referred to as adatoms, with nine bare MXenes surfaces are discussed. To facilitate the analysis the present study is restricted to MXenes with M_2C stoichiometry where M corresponds to a d^2 (Ti, Zr, Hf), d^3 (V, Nb, Ta), and d^4 (Cr, Mo, W) TMs.

7.1. GEOMETRY AND STABILITY OF TM@MXENES

The interaction of adatoms on each (0001) MXene surfaces has been investigated by considering four different high symmetry sites, see Figure 3, denoted as top (T) site when the adatom is placed above an M surface atom; bridge (B) site, sited above the surface in the midpoint of a M-M bond; and metal, H_M, and carbon, H_C, three-fold hollow sites with either a metal or a carbon atom lying beneath. Such calculations were carried out firstly at PBE level, and then, for the obtained minima, reoptimized at PBE-D3 level. Overall, this implied over 1000 optimizations.

In any case, most of bridge sites relaxed towards H_M or H_C. Indeed, H_M is the most common and preferred site, followed by H_C site for the vast majority of TM@MXene configurations. There exists just one single situation where the top site is the most stable, which is Cd@Zr_2C, and five configurations where the B site is found to be a minimum: Y@Ti_2C, Zr@Ti_2C, Cd@Hf_2C, Rh@Cr_2C, Ag@Cr_2C, and Cd@Cr_2C. To get more insight, the adsorption strengths are discussed in the next section.

7.2. ADSORPTION ENERGY

In a first step, the E_{ads} PBE-D3 values for 4*d* TMs on the (0001) basal surface of the explorer MXenes were acquired and listed in Table 1. Note in passing by that PBE E_{ads} values are just slightly less strong, being in average terms, 0.3 – 0.4 eV smaller. In any case, as one can notice, the adsorption energies in Table 1 range from 1 to 10 eV, and normally are quite large, except for Cd adatoms on light MXenes (Ti_2C, Zr_2C, Hf_2C, and V_2C), where such an interaction could be

catalogued as physisorption. However, for the rest, the interaction is strong, being largest for Mo, Tc, Ru, and Rh adatoms supported on Cr_2C, Mo_2C, and W_2C. From the above, it is clear that the adsorption strength depends on both the M_2C M adatoms, and the TM adaoms.

E_{ads} TM@M_2C [eV]											
	M\TM	**Y**	**Zr**	**Nb**	**Mo**	**Tc**	**Ru**	**Rh**	**Pd**	**Ag**	**Cd**
d^2	**Ti**	2.77	3.67	3.79	5.76	4.37	5.01	5.02	3.16	1.52	0.31
	Zr	2.59	3.39	3.35	5.56	3.86	4.79	5.11	3.44	1.60	0.32
	Hf	3.36	4.21	4.18	6.42	4.79	5.74	6.04	4.29	2.29	0.49
d^3	**V**	3.09	4.16	4.08	6.48	4.56	4.63	4.26	2.49	1.18	0.43
	Nb	4.52	5.71	5.58	7.96	6.21	6.49	6.27	4.47	2.78	1.26
	Ta	2.64	3.83	3.65	6.04	4.33	4.68	4.52	2.69	0.87	1.07
d^4	**Cr**	5.21	6.62	6.59	8.57	6.29	5.96	5.74	4.19	2.67	1.54
	Mo	6.52	7.95	7.93	9.93	7.61	7.42	7.03	5.46	4.12	2.77
	W	7.08	8.59	8.69	10.78	8.79	8.38	7.89	6.29	4.59	3.07

Table 1.PBE-D3 E_{ads} of all TM@M_2C configurations.

One can evaluate the E_{ads} of the different TMs along the 4*d* series, as done in Figure 4. Notice the volcano shape of the trend, with an increase up to Mo, followed by a decrease up to Cd. This goes along with the number of unpaired *d* electrons; this is, the E_{ads} increases with the number of *d* electrons, reaching a maximum at d^5 half-filled configurations, like in the Mo $4d^5$. From this on, the pairing of electrons provokes a decrease in the E_{ads} value, up to the Cd filled $4d^{10}$ configuration.

To further investigate the SAC isolation or the thermodynamic trends towards clustering or isolation, the PBE TM bulk cohesive energy of each metal has been gained, [41] and so the E_{diff} has been obtained. Thus, for those cases with E_{diff} >0 there would be a thermodynamic driving force towards adatom isolation, while E_{ads} <0 would go towards clustering. However, one should regard that DFT has an intrinsic error, of *ca.* 0.2 eV. Therefore, E_{diff} values within this error range, should not be assigned neither as favourable SACs nor like clusters. Table 2 is a compilation of the different cases where this happens, mostly cases for Mo and Ag adatoms, and the Hf_2C MXene, followed by Nb_2C and Cr_2C.

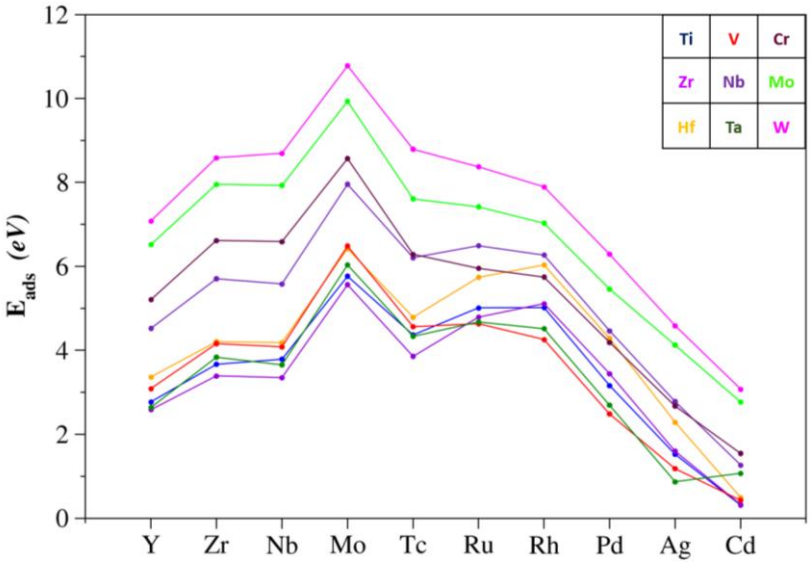

Figure 4. Evolution of the PBE-D3 E_{ads} along the 4*d* series for all the considered M_2C MXenes.

Adatom (M)	MXene (M_2C)	E_{diff} [eV]
Pd	Zr_2C	-0.27
Mo	Hf_2C	0.21
Ag	Hf_2C	-0.20
Cd	Hf_2C	-0.24
Mo	V_2C	0.27
Ru	Nb_2C	-0.18
Ag	Nb_2C	-0.29
Mo	Ta_2C	-0.17
Rh	Cr_2C	0.12
Ag	Cr_2C	0.18

Table 2. PBE E_{diff} of all the cases with unclear isolated atom or clustering preferences.

One can plot E_{diff} along the *d* series, as done on Figure 5 where it appears that as one goes along the *d* series, the adsorption energy increases in analogy the adsorption strength increases by moving down the period, as shown in Figure 6. As far as *d* series is concerned, is observed on all MXenes that the elements with an empty or full occupancy of the 4*d* shell, *e.g.*, Y and Cd,

would display the smallest cohesive energies, which are placed at the extremes of the volcano shape. According to this, one would expect such TMs to have the largest E_{diff}, and, as one moves away from these values the E_{diff} would decrease, so the E_{diff} representation should have a concave tendency in principle. However, this trend is not observed, and, on the contrary, a zigzag shape is observed. The clearest exception of this trend is Ta_2C, which has lower adsorption energy than Hf_2C and Nb_2C, as shown in Figures 5 and 6. Thus, Ta_2C can be considered as an out-layer that has less appetence for isolated atoms.

Indeed, there is a trend with the first elements with a low occupancy of *d* shell, where the adatoms with an empty or semi-empty half-shell seems to follow the trend of a strong field situation. With the Y adatom, there is just one electron in the half-shell, so it is not semi-full and has less stability; with Zr, there are two electrons in the half-shell, so there is more stability, and therefore, the TM@MXene has higher E_{ads}. In the case of Nb adatom, there are three electrons, two placed in the same orbital with opposite spins and one unpaired in another orbital, so the half-shell will have a high electron repulsion, higher that the other adatoms mentioned above, and so, lower stability, and higher E_{ads}. The last adatom that follows this trend is Mo, which has the half-shell occupied by four electrons, distributed within the two orbitals, and that would be reflected in a higher E_{ads}. From this adatom on, this trend losses strength as the higher half-shells gains electrons, and so the field seems to get distorted.

So, following Figure 5, it can be said that Zr adatom can be isolated within all the explored MXenes, where other TMs, such as Nb, are difficult to isolate regardless the MXene. For the rest of cases, intermediate situations are found that depend on both the employed M_2C and the TM adatom. For instance, W_2C and Mo_2C are signatures of TM dispersion, while few SACs are possible on Zr_2C, expect for Zr adatoms upon.

From the above, we can summarize that the adatoms with less than half occupancy 4*d* shell follow the strong field situation trend, while the ones with more than half occupancy 4*d* shell follow the concave tendency as expected from the E_{coh} valance.

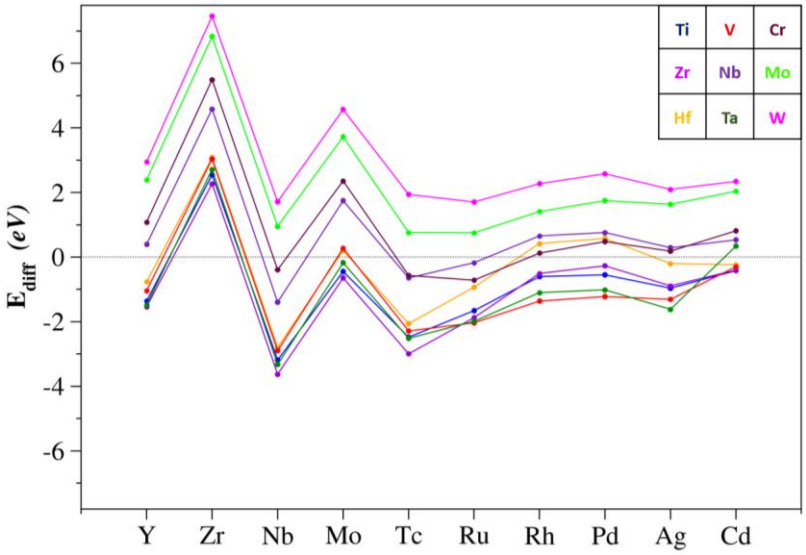

Figure 5. E_{diff} evolution along the 4*d* series of adatoms of the different studied MXenes.

Having analysed the 4*d* series trend, one can pay attention to the MXene substrate effects. For instance, Figure 6 shows the 4*d* trends separately for group IV and VI MXenes. The E_{diff} of the IV group increases moving down the period; the distance between the E_{diff} of Zr_2C and the Ti_2C MXenes is bigger than the one between Hf_2C and Zr_2C MXenes, as shown in Figure 6 on the left. There are few adatoms, Rh, Pd, and Ag, that do not follow this trend. In Zr_2C MXene, the E_{diff} of the mentioned adatoms is lower than the ones of Ti_2C MXene. In the V group, there exists a clear tendency going down the period, between the V_2C and the Nb_2C as the distance between both is proportional for all the adatoms, with little difference for the adatoms that have half occupancy 4*d* shell. Ta_2C, as mentioned earlier, is an outlier, which has similar E_{diff} behaviour to the one of V_2C. In this case, the Ru, Rh, Pd, and Cd are the adatoms that follow a similar situation observed with the Ti_2C and Zr_2C as mentioned earlier. The E_{diff} values of these adatoms on the Ta_2C MXene are higher than the ones for V_2C. Concerning the VI group, Figure 6 on the right, the E_{diff} increases as going down the period, the distance between the E_{diff} of Mo_2C and the W_2C MXenes is smaller than the one of Cr_2C and Mo_2C MXenes, a trend contrary to group IV. All the adatoms follow this trend with the exception of Ag and Cd adatoms. With W_2C MXene, the adatoms mentioned have a lower E_{diff} compared with the trend of all the adatoms as shown in the right panel of Figure 6.

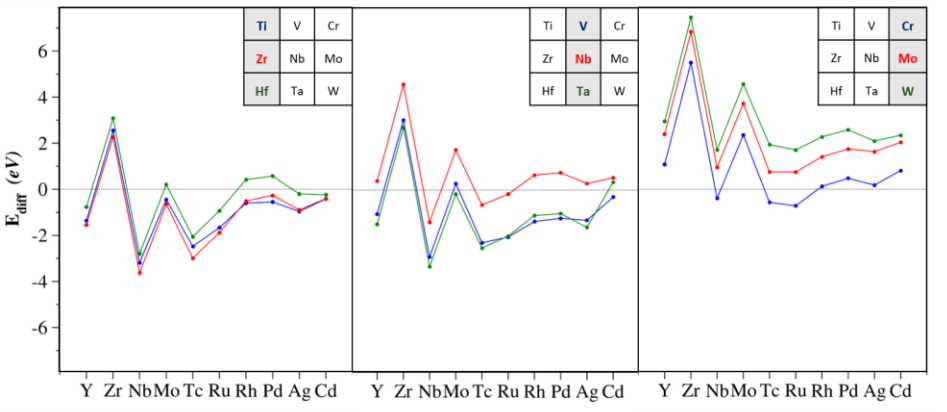

Figure 6. E_{diff} trend of the MXenes along the groups IV to VI.

These trends are more pronounced going through the series. For instance, in the 3*d* series, see Figure 7 on the left, the E_{diff} increases going along the series, the E_{diff} distance between V_2C and Ti_2C MXenes is smaller than the one between Cr_2C and V_2C MXenes. Note that there are a few adatoms, Ru, Rh, Pd, and Ag, that do not follow this trend. On V_2C MXene, such exceptional adatoms have a lower E_{diff} than the ones of Ti_2C MXene, a similar situation is observed between the Zr_2C and the Ti_2C MXenes. Concerning the 4*d* series, middle panel of Figure 7, the E_{diff} distance between the same adatoms of the different MXenes is proportional, with a little variation with the adatoms that have half occupancy *4d* shell. The trend is regular on 3*d* and 4*d* series, but, on 5*d* series, see Figure 7 on the right, Ta_2C is an outlier again, displaying E_{diff} values consistently smaller than expected. The unique configuration that differs is that just Cd@Ta_2C MXene, which has a higher E_{diff} than Cd@Hf_2C.

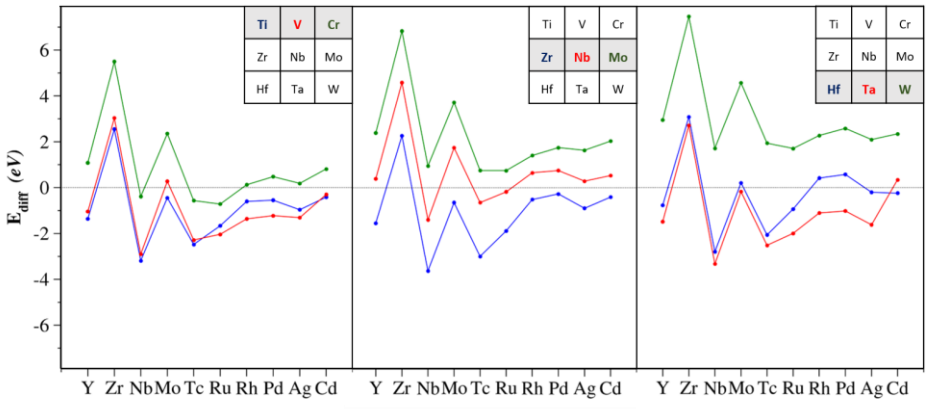

Figure 7. E_{diff} trends for the studied MXenes 3*d* (left), 4*d* (middle), and 5*d* (right) series.

7.3. ADATOM-MXENE – DISTANCES

The distances between the MXene surface metal atoms and the *d*-block element adatom could be a structural factor when studying the E_{ads} of the different adatoms attached to MXenes. One may argue that the smaller the distance between the adatom and the MXene, the stronger is the chemical bond and, consequently, the E_{ads} would be more favourable. To this end, the adatom height with respect the MXene surface plane, *h*, has been gained, and the adatoms trend follows a convex trend, as shown in Figure 8, just the opposite of the volcano plot shown in Figure 4; *i.e.,* the stronger the bonding, the smaller the height.

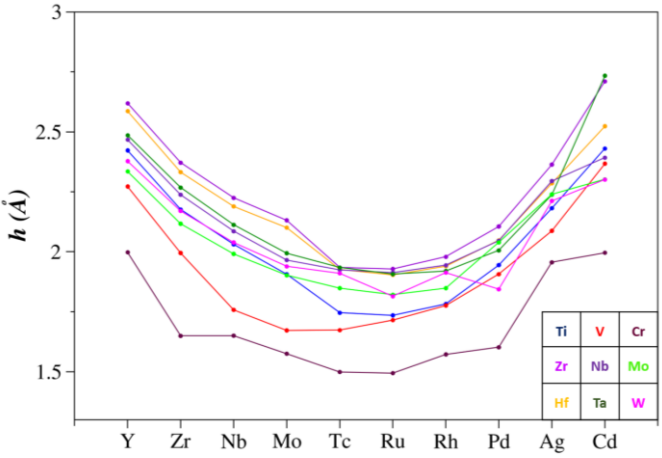

Figure 8. Trend of the adatom height, *h*, to the MXene surface along the 4*d* series.

To further support the previous statement, one can correlate the height of the different adatoms versus the TM@MXene adsorption energy, as shown in Figure 9. When doing so, the trend of the larger the E_{ads}, the smaller the height, h, is consistently observed. However, the adjustment is limited, this is, having regression coefficient R^2 values always below 0.67, as shown in Figure 9. This implies that the height is biased by the adsorption strength, but not just governed by that single factor, and other factors must apply. Indeed, the linear adjustment is best for V_2C, but decreases when going down a group and along a *d* series, for instance, affected by the strong field situation for those TMs with less than half 4*d* occupancy that follow a strong field situation.

As going down the period and along with the series, the R^2 decreases as observed along the sequences V_2C, Nb_2C and Ta_2C group, and Zr_2C, Nb_2C, and Mo_2C series, respectively. It can be said that, in the third period, there is a relation between the E_{ads} and the height from the MXene surface to the adatom, but this relation gets less clear as going down the period and through the series.

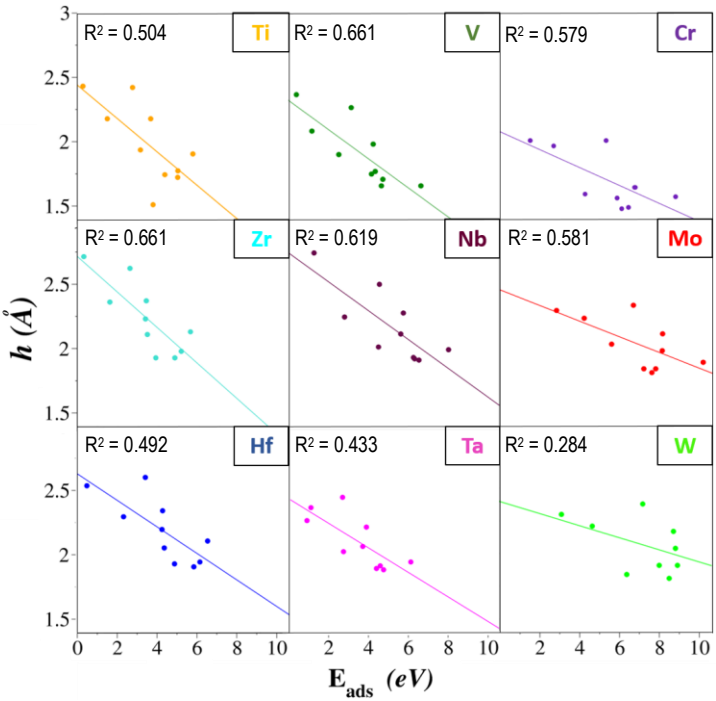

Figure 9. Linear correlation of heights, h, versus the TM adatom E_{ads}.

7.4. ADSORPTION ENERGY VS EXFOLIATION ENERGY

It is reasonable to think it could exist a certain relationship between the reactivity of the synthesized MXene and its exfoliation energy. This hypothesis would imply that MXenes with high exfoliation energies will be less stable, and therefore, more chemically active, and more prone to have a TM@MXene situation than those with lower exfoliation energies. This is shown correlating its adsorption energies for each TM with respect the exfoliation energies, taken from the Al-containing MAX phases, and computed using the same procedure as here used[43].

Notice that, Figure 10, the *x*-axis, contains the E_{exf} of the Al@MAX phases, and so are the same values for all the graphs, while the *y*-axis, displays the TM@MXene E_{ads} of each adatom anchored on the nine MXenes. Accordingly, one should take notice of the variation between the graphs of the ordinate axis, the height of the points of the graphs, and in consequence, the slope when doing a regression.

Concerning the adatoms, as going through the series, the TM@MXene/Al@MAX relation increases till the Mo@MXene and then decreases until Cd@MXene. As expected, the E_{ads} is affected by the E_{exf}, so that the larger the exfoliation energy, the larger the adsorption energy. Aside, and as above stated, the slope increases up to Mo, and then decrease until Cd, a feature that could be explained based on the full shell model, as, while the TM shell is getting completed, the slope decrease, implying that a less activity is observed. Thus, based on such hypothesis, the Mo adatoms are the ones best targeted for SAC situation, closely followed by Tc and the Nb adatoms.

Secondly, the contribution within each TM is analyzed. Overall, one may conclude that all cases follow a similar trend. However, one has to remark two exception cases: V_2C and Ta_2C MXenes, which both have a higher E_{exf} and a lower E_{ads} compared to Nb_2C, and contrary, Mo_2C MXene has a lower E_{exf} and a higher E_{ads} compared to Cr_2C and W_2C. The fact that the relation E_{ads} versus E_{exf} tends to increase as going through the different MXenes implies that as going through the period and along the series of the *d*-metal of the MXene, the substrate implication is more favourable for SAC.

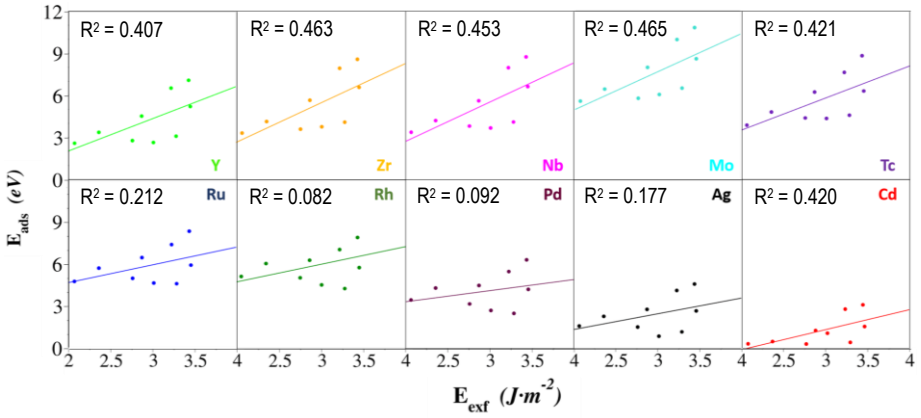

Figure 10. Trends of E_{ads} of TM@MXene versus E_{exf} of Al containing MAX.

It can be said as well that the W_2C MXene is the one that has the most favourable SAC situation, followed by Mo_2C, Nb_2C, Hf_2C, and Zr_2C, respectively. Getting these results, one can conclude that, in this case, the *d*-metal MXene acts better as a substrate once the *d*-metal has a higher number of valence electrons, as farther are these from the nuclei.

In Figure 10 are shown the values obtained from the linear fitting of each trend. Noting that, R^2 increases moving from the full shell towards the half-full shell, with two exceptions: *(i)* Nb adatom has a smaller R^2 than Zr, and *(ii)* Ag and Cr adatoms that have a higher R^2 than expected.

In short, one can conclude that the best MXene for a SAC situation is that one in which the *d*-metal is characterized by a higher number of valence electrons, which are farther from the nuclei and available to bond the TM adatoms. Concerning the adatoms, the half-full shell situation is the most appropriate for the TM adatom. Attending to this, Mo adatom, followed by Tc and Nb, are the best ones. Clearly, E_{exf} is relevant factor to identify the reactivity of MXenes but is not the only one, as one can observe from the regression coefficient in Figure 10.

7.5. Comparison among Adatoms from Different Series

The above SAC is definitely complex ant it is to be expected that just one substrate will not work with the same accuracy for all the different metal atoms. In this section, the trends for isolating or clustering between 3*d* and 4*d* adatoms are compared, using as substrate the MXenes. This will lead us to capture interesting trends when moving down the *d* series along the groups.

Figure 11 shows a E_{diff} comparison between 3*d* adatoms and 4*d* adatoms belonging to the same group, *versus* the metal composition of MXenes. At first glance, 4*d* Zr and Mo adatoms are generally better isolated on the MXene surfaces, compared to the respective 3*d* Ti and Cr adatoms of the same respective groups. In all the cases, Nb_2C, Cr_2C, Mo_2C, and W_2C MXenes display higher E_{diff} values with the 4*d* adatoms compared to the corresponding 3*d* adatoms. In the case of Hf_2C MXene, the Tc, Ru, Rh, and Pd, 4*d* adatoms have higher E_{diff} than the counterparts Mn, Fe, Co, and Ni 3*d* adatoms. The rest of adatoms that have not been mentioned, have a higher E_{diff} with the 3*d* rather than the 4*d*.

In conclusion, there are a few 4*d* adatoms that can be energetically isolated with the investigated MXenes. As going from the 3*d* to the 4*d* adatoms, d^4 MXenes act better as a substrate with the 4*d* metal atoms rather than the 3*d*. The Zr and Mo 4*d* metal atoms have more tendency to be as a SA with the studied MXenes than Ti and Cr 3*d* metal atoms, respectively.

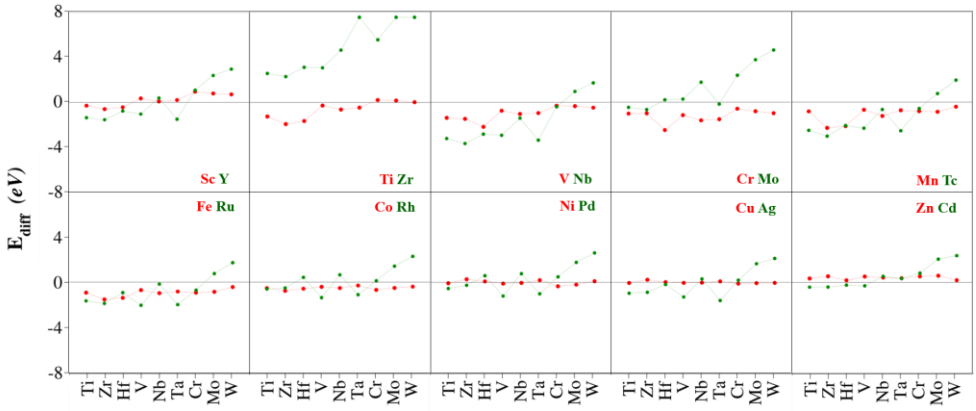

Figure 11. Trends of E_{diff} 3*d* and 4*d* adatoms on the nine explored MXenes.

7.6. Pt-Group

Given the possibilities of isolating Ru, Rh, and Pt-group metals on a series of MXenes mostly Nb_2C, Cr_2C, Mo_2C, and W_2C, plus the same casuistry of Ag coinage metal, one may wonder whether such trends to isolate Pt-group and coinage metals are also featured on 5*d* TMs. Thus, the six Pt-group TMs, these are the Ru, Rh, Pd, Ps, Ir, and Pt are studied in this section, plus Ag and Au. The exploration has been carried out solely on H_M and H_C sites, as being the only minima found for the 4*d* Pt-group TMs and Ag, resulting the H_M the most common preferred site, with only few TM@MXene cases preferring the H_C site.

The corresponding E_{diff} values comparing 4*d* and 5*d* TMs is shown in Figure 12, revealing similar trends for the 5*d* TM, where is worth pointing out that, while 4*d* Ru and Rh adatoms have larger E_{diff} values than respective 5*d* Os and Ir with the sole exception of V_2C, 4*d* Pd and Ag adatoms display smaller E_{diff} values than the 5*d* Pt and Au counterparts. The results are translated into the fact that Pt and Au adatoms are easier to isolate than the Os and Ir adatoms, plus all the 5*d* elements are more prone to be as a SA with the V_2C MXene.

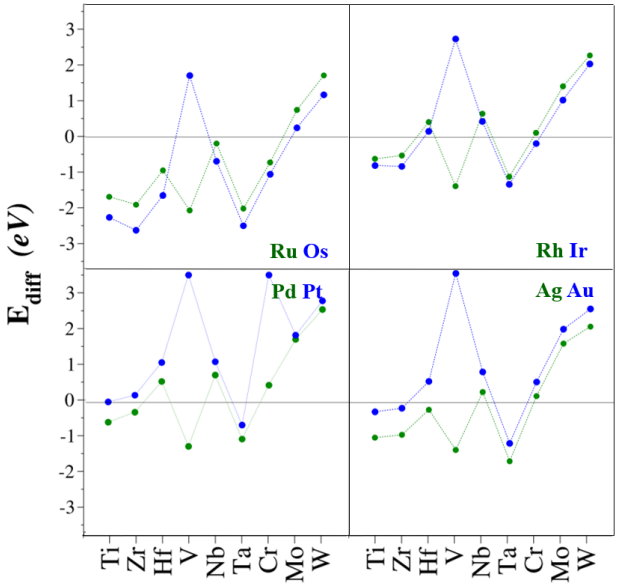

Figure 12. Evolution of E_{diff} for the different studied MXenes comparing 4*d* and 5*d* TMs.

Another captured trend is the adatom height evolution versus E_{ads}, see Figure 13. Ideally, one would expect a similar regression slope, but with a larger height for 5*d* TMs given their larger atomic radii. However, 5*d* TMs display a smaller slope, and as a general trend, have a smaller height to the MXene and a larger E_{ads}, than the 4*d*.

Figure 13 has also the compilation of the R^2 values obtained from the linear fitting of each. Noting that the 4*d* R^2 values are larger than the 5*d*, it can be said that as going down a group the dispersion increases. This could be because as ones goes down the period, the valence electrons are more delocalized, thus, its height and E_{ads} vary more from one value to another.

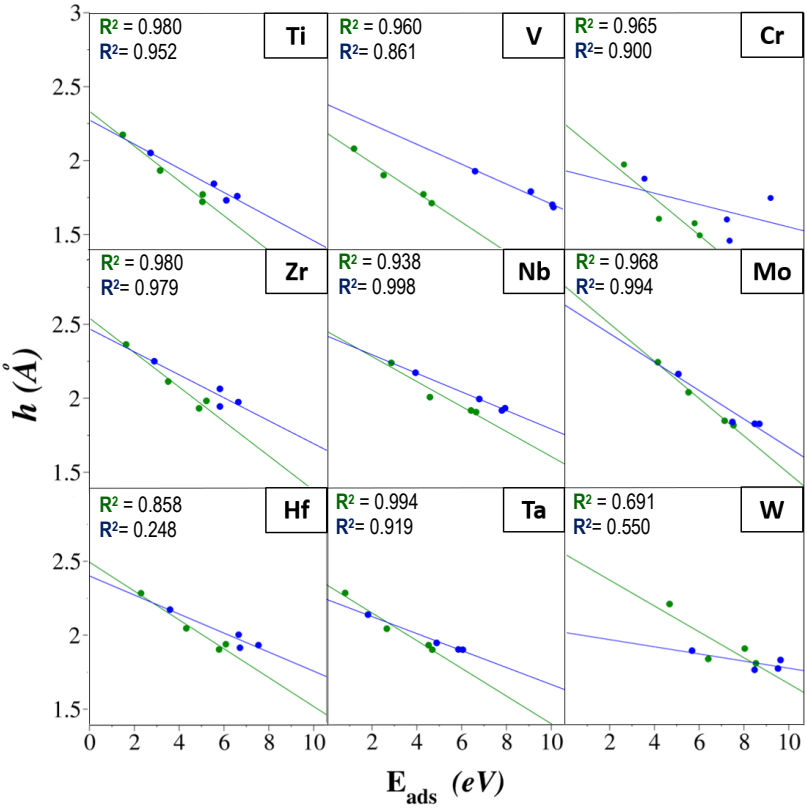

Figure 13. Correlation of TM heights, *h*, *versus* their E_{ads}.

8. CONCLUSIONS

Once studied the adsorption energy on the different TMs on the different MXenes, the following conclusions can be extracted:

- The preferred site for the 4*d* TM adatoms on the MXenes is H_M site, followed by H_C.
- Zr_2C is apparently able to isolate any 4*d* TM adatom upon.
- The adatoms with less than half occupancy 4*d* shell seem to follow the strong field situation trend and the ones with more than half occupancy 4*d* shell seem to follow a concave tendency.
- There is a relation between the TM height and the E_{ads} as far as the stronger the bond, the closer the adatom to the MXene surface. However, this relation gets less clear as going down the groups and through the *d* series.
- The best MXene for a SAC situation is one with a high number of valence electrons and radius, which is the case for W_2C.
- As far as TM adatoms are concerned, the half-full d shell situation is the most appropriate for a SAC, as featured by Mo.
- Clearly, the MAX exfoliation energy is a physicochemical descriptor biasing the MXene surface chemical activity, here shown for the E_{ads}.
- When going down to the 5*d* TMs, it appears as late TMs are better dispersed, as observed comparing Pt and Au versus Pd and Ag.
- All the 5*d* elements are more prone to be as a SA with the V_2C MXene.

9. REFERENCES AND NOTES

1. Ertl, G. Wilhelm Ostwald: Founder of Physical Chemistry and Nobel Laureate 1909. *Angew. Chem. Int. Ed.* **2009***, 48*, 6600−6606.
2. Ma, Z.; Zaera, F. Heterogeneous Catalysis by Metals. In Encyclopedia of Inorganic Chemistry; King, R. B., Ed.; Wiley*: New York* **2005**, 1768−1784.
3. Busca, G. Heterogeneous Catalytic Materials. *Elsevier: Amsterdam*, **2014**, 23−35.
4. Morales-García, Á.; Calle-Vallejo, F.; Illas, F. MXenes: New Horizons in Catalysis. *ACS Catal*. **2020**, *10*, 13487-13503.
5. Naguib, M.; Kurtoglu, M.; Presser, V.; Niu, J.; Heon, H.; Hultman, L.; Gogotsi, Y.; Barsoum, M.V. Two-Dimensional Nanocrystals Produces by Exfoliation of Ti_3AlC_2. *Adv. Mater*. **2011**, *23*, 4248-4253.
6. Darby, M.T.; Stamatakis, M.; Michaelides, A.; Sykes E. C. Lonely Atoms with Special Gifts: Breaking Linear Scaling Relationships in Heterogeneous Catalysis with Single-Atom Alloys. *J. Phys.Chem*. Lett. **2019**, *10*, 3129-3133
7. Huang, B.; Neng, L.; Ong, W.J.; Zhou, N. Single Atom-Supported MXene: How Single-Atomic-Site Catalysts Tune the High Activity and Selectivity of Electrochemical Nitrogen Fixation. *J.Mater. Chem*. A. **2019**, *7*, 27620-27631.
8. Alhabeb, M.; Maleski, K.; Anasori, B.; Lelyukh, P.; Clark, L.; Sin, S.; Gogotsi, Y. Guideline for Synthesis and Processing of Two-Dimensional Titanium Carbide (Ti3C2Tx MXene). *Chem. Mater*. **2017**, *29*, 7633−7644.
9. Ramalingam, V.; Varadhan, P.; Fu, H.C.; Kim, H.; Zhang, D.; Chen, S.; Song, L.; Ma, D.; Wang, Y.; Alshareef, H.N.; He, J.H. Heteroatom-Mediated Interactions between Ruthenium Single Atoms and an MXene Support for Efficient Hydrogen Evolution. *Adv. Mater*. **2019**, *31*, 1903841.
10. Thomas, J. M.; Raja, R.; Lewis, D. W. Single-site heterogeneous catalysts. *Angew. Chem. Int. Ed.* **2005***, 44*, 6456–6482.
11. Yang, X.F.; Wang, A.; Qiao, B.; Li, J.; Liu, J.; Zhang, T. Single-Atom Catalysts: A New Frontier in Heterogeneous Catalysis. *J. Am. Chem. Soc.* **2013**, *46*, 1740-1748.
12. Qiao, B.; Wang, A.; Yang, X.; Allard, L. F.; Jiang, Z.; Cui, Y.; Liu, J.; Li, J.; Zhang, T. Single-Atom Catalysis of CO Oxidation Using Pt1/ FeOx. *Nat. Chem.* **2011**, *3*, 634−641.
13. Chen, Y.; Ji, S.; Chen, C.; Peng, Q.; Wang, D.; Li, Y. Single-Atom Catalysts: Synthetic Strategies and Electrochemical Applications. *Joule* **2018**, *2*, 1242-1464.
14. Skrzypczyk, P.; Short, A.J.; Popescu, S. Work Extraction and Thermodynamics for Individual Quantum Systems. *Nat. Commun*. **2014**, *5*, 4185.
15. Manadé, M.; Viñes, F.; Illas, F. Transition Metal Adatoms on Graphene: A Systematic Density Functional Study, *Carbon* **2015**, *95*, 525-534.
16. Kim, S.; Puigdollers, A.R.; Gamallo, P.; Viñes, F. Functionalization of γ-Graphyne by Transition Metal Adatoms. *Carbon* **2017**,*120*, 63-70.
17. Gupta, V.P. Principles and Applications of Quantum Chemistry. *Ac. Press* **2016**, *2*, 1-46.
18. Gupta, V.P. Principles and Applications of Quantum Chemistry. *Ac. Press* **2016**, *2*, 47-62.
19. Sholl, D.; Steckel, J.A. Density Functional Theory: A Practical Introduction. *Willey* **2011**.
20. Gupta, V.P. Principles and Applications of Quantum Chemistry. *Ac. Press* **2016**, *2*, 155-194.
21. Kamysbayev, V.; Filatov, A. S.; Hu, H.; Rui, X.; Lagunas, F.; Wang, D.; Klie, R. F.; Talapin, D. V. Covalent Surface Modifications and Superconductivity of Two-Dimensional Metal Carbide MXenes. *Science* **2020***, 369*, 979.

22. Paniagua, J.C.; Alemany, P. Química Quàntica. *Llibres de l'Índex* **2000**, 2-3.
23. Born, M.; Oppenheimer, R. Zur Quantentheorie Der Molekeln. *Ann. Phys*. **1927**, *389*, 457-484.
24. Borlido, P.; Aull, T.; Huran. A.W.; Tran, F.; Marques, M.A.; Botti, S. Large Scale Benchmark of Exchange-correlation Functionals for the Determination of Electronic Band Gaps of solids. *J. Chem. Theory. Comput.* **2019**, *15*, 5069-5079.i, C. Atoms, Molecules, Solids, and Surfaces: Applications of the Generalized Gradient Approximation for Exchange and Correlation. *Phys. Rev. B* **1992**, *46*, 6671-6687.
25. Tsuzuki, S; Lüthi, H.P. Interaction Energies of van der Waals and Hydrogen Bonded Systems Calculated Using Density Funcional Theory: Assessing the PW91 Model. *J. Chem. Phys.*, **2001**, *114*, 3949.
26. Hammer, B; Hansen, L.B.; Nørskov, J. K. Improved Adsorption Energetics within Density-Functional-Theory Using Revised Perdew-Burke-Ernzerhof Funcionals. *Phys. Rev*. **1999**, *59*, 7413-7421.
27. Politi, J. R. S.; Viñes, F.; Rodríguez, J.A.; Illas, F. Atomic and Electronic Structure of Molybdenum Carbide Phases: Bulk and low Miller-Index Surfaces. *Phys. Chem. Chem. Phys*. **2013**,*15*, 12617-12625
28. Gouveia, J. D.; Viñes, F.; Illas, F.; Gomes, J.R.B., MXene Atomic Layer Stacking Phase Transitions and their Chemical Activity Consequences. *Phys. Rev. Mat*. **2020**, *4*, 054003.
29. Morales-Salvador, R.; Morales-Garcia, Á. Two-Dimesional Nitrides as Highly Efficient Potential Candidates for CO_2 Capture and Activation. *Phys. Chem*. *Chem. Phys*. **2018**, *20*, 17117-17124.
30. Towler, M.; Zupan, A.; Causà, M. Density Functional Theory in Periodic Systems Using Local Gaussian Basis Sets. *Comput. Phys. Commun*. **1996**, *98*, 181-205.
31. Naguib, M.; Gogotsi, Y. Synthesis of Two-Dimensional Materials by Selective Extraction. *Acc. Chem. Res*. **2015**, *48*, 128-135.
32. Naguib, M.; Mochalin, V.N.; Barsoum, M.W.; Gogotsi, Y. 25th Anniversary Article: MXenes; A New Family of Two-Dimensional Materials. *Adv. Mater*. **2014**, *26*, 996-1005.
33. Zhang, X.; Lei, J.; Wu, D.; Zhao, X; Jing, Y.; Zhou, Z. A Ti-anchored Ti_2CO_2 Monolayer (MXene) as a Single-Atom Catalyst for CO Oxidation. *J. Mater. Chem*. A. **2016**, *13*,4871-4878.
34. Zhao, D.; Chen, Z.; Yang, W.; Liu, S.; Zhang, X.; Yu, Y.; Cheong, W.C.; Zheng, L.; Ren, F.; Ying, G.; Cao, X.; Wand, D.; Peng, Q.; Wang, G.; Chen, C. MXene (Ti_3C_2) Vacancy-Confined Single-Atom Catalyst for Efficient Functionalization of CO_2. *J. Am. Chem. Soc*. **2019**, *141*, 4086-4093.
35. Grimme, S.; Hansen, A.; Brandenburg, J.vG.; Bannwarth, C. Dispersion-Corrected Mean-Field Electronic Structure Methods. *Chem. Rev*. **2016**, *116*,5105-5154.
36. Sato, T.; Tsuneda, T.; Hirao, K. Van der Waals Interactions Studies by Density Functional *Theory. Mol. Phys*. **2005**, *103*, 1151-1164.
37. Berland, K.; Cooper, V. R.; Lee, K.; Schröder, E.; Thonhauser, T.; Hyldgaard, P.; Lundqvist, B. Van der Waals Forces in Density Funcional Theory: A Review of the vdW-Method. *Rep. Prog. Phys.* **2015**, *78*, 066501.
38. Xu, P.; Alkan, M.; Gordon, M. S. Many-Body Dispersion. *Chem. Rev*. **2020**, *120*, 12343-12356.
39. Grimme, S.; Antony, J.; Ehrlich, S.; Krieg, H. A Consistent and Accurate Ab Initio Parametrization of Density Functional Dispersion Correction (DFT-D) for the 94 Elements H-Pu. *J. Chem. Phys*. **2010**, *132*, 154104.
40. Janthon, P.; Luo, S.; Kozlov, S.; Viñes, F.; Limtrakul, J.; Truhlar, D.; Illas, F. Bulk Properties of Transition Metals: A Challenge for the Design of Universal Density Functionals. *J. Chem. Theory Comput.* **2014**, *10*, 3882-3839.
41. Gouveia, J.; Morales-Garcia, Á.; Viñes, F.; Gomes, J.; Illas, F. Facile Heterogeneously Catalyzed Nitrogen Fixation by MXenes. *ACS Catal.* **2020**, *10*, 5049-5056.
42. Dolz, D.; Morales-García, Á.; Viñes, F.; Illas, F. Exfoliation Energy as a Descriptor of MXenes Synthesizability and Surface Chemical Activity. *Preprints* **2020**, 2020120308.

43. Oschinsky, H.; Morales-García, Á.; Illas, F. Interaction of First Two Transition Metals with M_2C (M=Ti, Zr, Hf, V, Nb, Ta, Cr, Mo, W) MXenes: A Quest for Single-Atom Catalysts. *Under Review*.